PERGAMON

Computers and Structures 80 (2002) 235–255

Computers & Structures

www.elsevier.com/locate/compstruc

On the asymptotic behavior of shell structures and the evaluation in finite element solutions

Phill-Seung Lee, Klaus-Jürgen Bathe *

Department of Mechanical Engineering, Massachusetts Institute of Technology, 77 Massachusetts Avenue, Room 3-356, Cambridge, MA 02139, USA

Received 15 October 2001; accepted 4 December 2001

Abstract

The objective of this paper is to demonstrate how the asymptotic behavior of a shell structure, as the thickness (t) approaches zero, can be evaluated numerically. We consider three representative shell structural problems; the original Scordelis–Lo roof shell problem, a herein proposed modified Scordelis–Lo roof shell problem and the partly clamped hyperbolic paraboloid shell problem. The asymptotic behavior gives important insight into the shell load bearing capacity. The behavior should also be known when a shell problem is used to test a shell finite element procedure. We briefly review the fundamental theory of the asymptotic behavior of shells, develop our numerical schemes and perform the numerical experiments with the MITC4 shell finite element.

Keywords: Shells; Asymptotic behaviors; Finite element solutions

1. Introduction

Shells are three-dimensional structures with one dimension, the thickness, small compared to the other two dimensions. This geometric feature is used in shell analysis in several respects: to define the geometry of shell structures, only the 2D mid-surface and thickness need be defined, and to define the shell behavior, assumptions can be used. These assumptions specifically comprise that the normal stress through the thickness of the shell vanishes and that straight fibers originally normal to the mid-surface remain straight during the deformation of the shell.

The major difficulties of shell analysis arise because the thickness of a shell is small. Shell structures can show varying sensitivity with decreasing thickness, depending on the shell geometry and boundary conditions. For a deeper understanding of the load bearing capacity of a shell, it is therefore important to investigate the behavior of the shell as the thickness decreases.

It is well known that the behavior of a shell structure belongs to one of three different asymptotic categories: the membrane-dominated, bending-dominated, or mixed shell problems [1–5]. Recently, various theoretical studies regarding the asymptotic behavior of shell structures have been presented, see [4–9] and the references therein. Chapelle and Bathe [4,5] presented some fundamental aspects regarding asymptotic behavior of shell structures specific for the finite element analysis. Pitkäranta et al. [6–8] observed the asymptotic diversity and limit behavior of cylindrical shells with different support conditions using asymptotic expansions of the displacement and strain fields. Blouza et al. provided further results regarding the mixed asymptotic behavior of shell problems [9].

In spite of many theoretical studies on and the importance of the asymptotic behavior of shell structures, simple algorithms to evaluate the asymptotic behavior have not been proposed, and few numerical results demonstrating the asymptotic behavior have been published. The objective of this paper is to present such algorithms and apply them to three shell structural

* Corresponding author. Tel.: +1-617-253-6645; fax: +1-617-253-2275.

E-mail address: kjb@mit.edu (K.J. Bathe).

0045-7949/02/$ - see front matter
PII: S0045-7949(02)00009-3

problems, one from each of the fundamental categories mentioned above.

In the following sections of the paper, we first briefly review the fundamental theory of the asymptotic behavior of shell structures in linear analysis. We then develop some simple algorithms to evaluate this behavior and perform the asymptotic analysis of three shell structures that display fundamentally different asymptotic behaviors; the original Scordelis–Lo roof shell problem, a modified Scordelis–Lo roof shell problem, and the partly clamped hyperbolic paraboloid shell problem. The MITC4 shell finite element is used for these numerical experiments [10].

2. The asymptotic behavior of shells

As the thickness of a shell structure approaches zero, the behavior of the shell generally converges to a specific limit state. This phenomenon is called the asymptotic behavior of shells.

Bending action, membrane action and shearing action are three basic load-bearing mechanisms of shell structures. Therefore, shell structures under loading have three corresponding deformation energies, which are respectively called the bending strain energy, membrane strain energy and shear strain energy. Because the shear strain energy is negligible when the thickness is small, the strain energy of shells mainly consists of two parts: membrane strain energy and bending strain energy.

In the engineering literature, frequently, the problem is referred to as bending-dominated when the shell carries the applied loads primarily by bending action, and is referred to as membrane-dominated when the shell carries the applied loads primarily by membrane action. This is a somewhat loose categorization and a more precise way to categorize shell behavior can be used and is based on the asymptotic behavior of the structure as its thickness decreases [4–9].

The asymptotic behavior of a shell strongly depends on the geometry of the shell surface, the kinematic boundary conditions, and the loading. Previous studies provide some fundamental theoretical results regarding the asymptotic behavior of shells, but only few numerical results are available that show the actually reached asymptotic stress, strain and energy conditions.

2.1. Fundamental asymptotic theory

We consider the linear Naghdi shell model or Koiter shell model, for which the general variational form is

Find $U^\varepsilon \in \mathscr{V}$ such that

$$\varepsilon^3 A_\mathrm{b}(U^\varepsilon, V) + \varepsilon A_\mathrm{m}(U^\varepsilon, V) = F^\varepsilon(V), \quad \forall V \in \mathscr{V}, \tag{1}$$

where ε is the thickness parameter t/L (t is the thickness and L is the global characteristic dimension of the shell structure which can be the diameter or overall length), the bilinear form A_b represents the scaled bending energy, the bilinear form A_m represents, respectively, the scaled membrane energy for the Koiter shell model and the scaled membrane and shear energies for the Naghdi shell model, U^ε is the unknown solution (displacement field), V is the test function, $\mathscr{V}$ is the appropriate Sobolev space, and F^ε denotes the external loading. We recall that the bilinear forms A_b and A_m are independent of the thickness parameter ε.

To establish the asymptotic behavior as ε approaches zero, we introduce the scaled loading in the form

$$F^\varepsilon(V) = \varepsilon^\rho G(V), \tag{2}$$

in which ρ is an exponent denoting the load-scaling factor. It can be proven that $1 \leqslant \rho \leqslant 3$, see for example [5,9].

The following space plays a crucial role in determining what asymptotic behavior will be observed,

$$\mathscr{V}_0 = \{V \in \mathscr{V} | A_\mathrm{m}(V, V) = 0\}. \tag{3}$$

This space is the subspace of "pure bending displacements" (also called the subspace of "the mid-surface inextensional displacements"). Eq. (3) tells that all displacements in $\mathscr{V}_0$ correspond to zero membrane and shear energies. When the content of this subspace is only the zero displacement field ($\mathscr{V}_0 = \{0\}$), we say that "pure bending is inhibited" (or, in short, we have an "inhibited shell"). On the other hand, when the shell admits non-zero pure bending displacements, we say that "pure bending is non-inhibited" (we have a "non-inhibited shell"). The asymptotic behavior of shells is highly dependent on whether or not pure bending is inhibited.

The "pure bending is non-inhibited" situation (that is, the case $\mathscr{V}_0 \neq \{0\}$) frequently results in the bending-dominated state. Then the membrane energy term of Eq. (1) asymptotically vanishes and with $\rho = 3$, the general form of the bending-dominated limit problem is

Find $U^0 \in \mathscr{V}_0$ such that

$$A_\mathrm{b}(U^0, V) = G(V), \quad \forall V \in \mathscr{V}_0. \tag{4}$$

This limit problem holds only when the loading activates the pure bending displacements. If the loading does not activate the pure bending displacements, that is, we have

$$G(V) = 0, \quad \forall V \in \mathscr{V}_0, \tag{5}$$

then the solution of the shell problem does not converge to the limit solution of the bending-dominated case, and the theoretical asymptotic behavior is as for the inhibited case, but very unstable [4,5]. Namely, only a small perturbation in the loading that does not satisfy Eq. (5)

Table 1
The classification of shell asymptotic behaviors

Case	Loading	Category
Non-inhibited shell $\mathscr{V}_0 \neq \{0\}$	Loading activates pure bending displacements $\exists V \in \mathscr{V}_0$ such that $G(V) \neq 0$	(i) Bending-dominated
	Loading does not activate pure bending displacements $G(V) = 0, \quad \forall V \in \mathscr{V}_0$	(ii) Membrane-dominated or mixed but unstable
Inhibited shell $\mathscr{V}_0 = \{0\}$	Admissible membrane loading $G \in \mathscr{V}'_{\mathrm{m}}$	(iii) Membrane-dominated
	Non-admissible membrane loading $G \notin \mathscr{V}'_{\mathrm{m}}$	(iv) Mixed

will change the asymptotic behavior to the bending-dominated state.

Considering the "pure-bending is inhibited" situation (that is, the case $\mathscr{V}_0 = \{0\}$), we use the load-scaling factor $\rho = 1$ and provided the problem is well-posed obtain the limit problem of the membrane-dominated case in the space $\mathscr{V}_{\mathrm{m}}$. This space is larger than $\mathscr{V}$ because only bounded shear and membrane energies are considered. The general form of the membrane-dominated limit problem is

$$\text{Find } U^{\mathrm{m}} \in \mathscr{V}_{\mathrm{m}} \text{ such that}$$
$$A_{\mathrm{m}}(U^{\mathrm{m}}, V) = G(V), \quad \forall V \in \mathscr{V}_{\mathrm{m}} \tag{6}$$

and this problem is well-posed provided the loading G is in the dual space of $\mathscr{V}_{\mathrm{m}}$. The condition $G \in \mathscr{V}'_{\mathrm{m}}$ is directly equivalent to

$$|G(V)| \leqslant C\sqrt{A_{\mathrm{m}}(V, V)}, \quad \forall V \in \mathscr{V}_{\mathrm{m}} \tag{7}$$

with C a constant. Eq. (7) ensures that the applied loading can be resisted by membrane stresses only, and hence the condition $G \in \mathscr{V}'_{\mathrm{m}}$ is said to correspond to an "admissible membrane loading". If the loading is a non-admissible membrane loading ($G \notin \mathscr{V}'_{\mathrm{m}}$), we have an ill-posed membrane problem. The asymptotic state then does not correspond to membrane energy only, and the shell problem is classified as a mixed problem.

The asymptotic categories of shell behaviors are summarized in Table 1. Note that the asymptotic behavior of shells contains important information regarding the shell load carrying capacity. In order to accurately interpret the response of shell structures, it is essential to understand the diversity in asymptotic shell structural behaviors.

2.2. Geometrical rigidity

The asymptotic behavior of a shell problem depends on whether or not the shell is inhibited. For an inhibited shell, the membrane action renders the structure relatively stiff. Inhibited shells, overall, have a larger stiffness than non-inhibited shells. Whether a shell is inhibited depends on the shell geometry and the boundary conditions.

Mid-surfaces of shells are classified to be elliptic, parabolic, or hyperbolic surfaces depending on whether the Gaussian curvature is positive, zero or negative, respectively. The parabolic and hyperbolic surfaces have asymptotic lines, which are defined as lines in the directions corresponding to which there is zero curvature. The dotted lines shown in Fig. 1 are asymptotic lines.

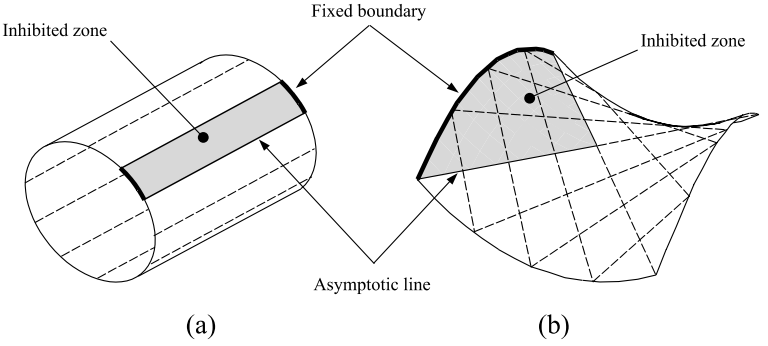

Fig. 1. The asymptotic lines and the inhibited zone (a) cylindrical surface, (b) hyperbolic surface.

The asymptotic lines and boundary conditions determine the inhibited zones of shells.

For example, Fig. 1(a) shows a cylindrical, that is, a parabolic surface. The asymptotic lines are parallel to the axial direction, and if we prescribe the displacements at the ends of the two cross-sections as shown in Fig. 1(a), the entire corresponding band (shaded region in Fig. 1(a)) becomes inhibited. The mid-surface of the Scordelis–Lo roof shell problem considered below is a parabolic surface.

We also consider below the partly clamped hyperbolic paraboloid shell problem shown schematically in Fig. 1(b). This is a hyperbolic surface and has two asymptotic directions. The boundary conditions result into the inhibited region shown in the figure.

2.3. Layers and characteristic length

The complete stress fields of shells are divided into global smooth components and various layer components. Layers are specifically due to discontinuities in geometry (curvature or thickness), incompatibilities of boundary conditions, and irregularities in the loading.

Fig. 2 shows three examples in which layers occur. In Fig. 2(a), the shell support and its boundary condition are compatible such that, assuming a pure membrane stress field in the shell, all equations of equilibrium are satisfied. On the other hand, the membrane forces alone cannot satisfy the conditions at the fixed boundary of Fig. 2(b). Such membrane incompatible boundary conditions like in Fig. 2(b) cause boundary layers, that is, localized edge effects inducing moments. Also, kinks and other discontinuities in shell geometries and irregularities of loadings as demonstrated in Fig. 2(c) and (d), disturb the membrane mode of shell behavior and induce stress layers, see for example [7,11–13].

Within stress layers of shells, the displacements vary rapidly and induce concentrations of strain energies. The width of layers can be classified by a characteristic length which is a function of two parameters: the shell thickness (t) and the overall length of the shell structure (L). Using dimensional analysis, the general form of the characteristic length is

$$L_c = Ct^{1-l}L^l, \tag{8}$$

in which l is a non-negative real number and C a constant. For example,

$$\begin{aligned} l &= 0 \Rightarrow L_c = Ct \\ l &= \frac{1}{2} \Rightarrow L_c = Ct^{1/2}L^{1/2} \\ l &= \frac{2}{3} \Rightarrow L_c = Ct^{1/3}L^{2/3} \\ l &= \frac{3}{4} \Rightarrow L_c = Ct^{1/4}L^{3/4} \\ &\vdots \end{aligned} \tag{9}$$

Eq. (8) shows that the shortest characteristic length is Ct which corresponds to $l = 0$, and the characteristic length is CL when $l = 1$. Ref. [7] discusses stress layers of various characteristic lengths considering cylindrical shells. We solve below for the stress layers in the Scordelis–Lo roof shell problem.

2.4. Load-scaling factor

As already noted, shell structures efficiently support applied external forces by virtue of their geometrical forms. Shells, due to their curvature, are much stiffer and stronger than other structural forms. For this reason, shells are sometimes referred to as "form resistant structures". This property means that the stiffness to weight ratio of a shell structure is usually much larger than that of other structural systems having the same span and overall dimensions. In this section, we briefly discuss the asymptotic stiffness of shell structures.

We stated in Section 2.1 that the asymptotic behavior of shells can generally be associated with just one real number, namely the load-scaling factor ρ, for which we have $1 \leqslant \rho \leqslant 3$.

In engineering practice, the information as to what load-scaling factor pertains to the shell considered is important for the design because the stiffness of the structure varies with ε^ρ. However, it is usually impossible to analytically calculate the proper load-scaling factor for a general shell problem. In this section, we

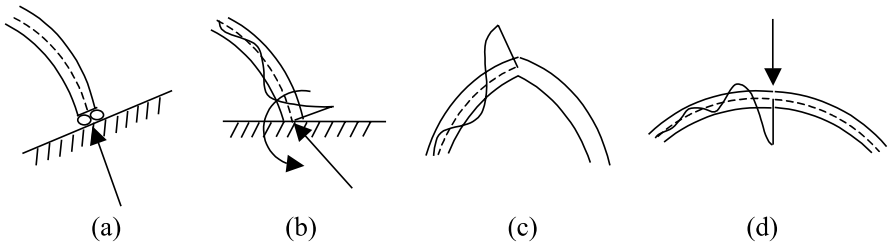

Fig. 2. Schematic regarding layers (a) membrane compatible boundary condition, (b) membrane incompatible boundary condition, (c) geometric discontinuity, (d) concentrated load.

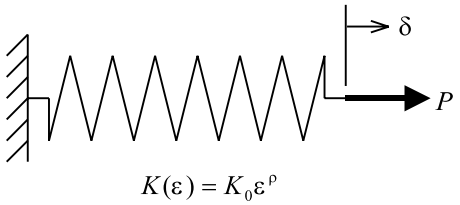

Fig. 3. Gedankenexperiment using a spring.

discuss some basic concepts to experimentally find the value through finite element solutions.

Consider the Gedankenexperiment shown in Fig. 3. The equilibrium equation of the model is

$$(K_0\varepsilon^{\rho}) \cdot \delta = P, \tag{10}$$

in which K_0 is a constant, ε is a thickness parameter, ρ is a scaling factor, P is the applied loading to the spring and δ is the displacement at the point of load application.

The strain energy of the model subjected to the scaled loading $P = P_0\varepsilon^{\mu}$ is

$$E(\varepsilon) = \frac{P^2}{2K(\varepsilon)} = \frac{P_0^2}{2K_0}\varepsilon^{2\mu-\rho}. \tag{11}$$

Note that the strain energy is a function of ε. Dividing $E(\varepsilon)$ by ε^{μ}, the scaled energy (E_0) is obtained:

$$E_0 = \frac{E(\varepsilon)}{\varepsilon^{\mu}} = \frac{P_0^2}{2K_0}\varepsilon^{\mu-\rho}. \tag{12}$$

Hence the scaled strain energy varies with $\varepsilon^{\mu-\rho}$. If the exponent μ of the applied scaled loading is larger than the appropriate load-scaling factor ρ, the scaled strain energy will asymptotically vanish as $\varepsilon \to 0$. If μ is smaller than ρ, the scaled strain energy will blow up. The condition that the scaled strain energy does not approach infinity or zero and be a constant value, that is $(P_0^2/2K_0)$, is that the exponent μ of the applied scaled loading be equal to the appropriate load-scaling factor ρ. This is an important observation in order to identify the appropriate load-scaling factor of arbitrary shell problems.

Applying a constant loading ($\mu = 0$ in Eq. (11)), we obtain the strain energy as a function of ε only and have

$$\log(E(\varepsilon)) = \log\left(\frac{P_0^2}{2K_0}\right) - \rho\log(\varepsilon). \tag{13}$$

This equation shows that the proper load-scaling factor ρ of the considered shell problem is nothing but the slope in the log E to log ε graph. This feature can also be used to find the proper load-scaling factor of arbitrary shell problems.

The strain energy of the general shell problem considered in Eq. (1) is

$$E(\varepsilon) = \tfrac{1}{2}[\varepsilon^3 A_{\mathrm{b}}(U^{\varepsilon}, U^{\varepsilon}) + \varepsilon A_{\mathrm{m}}(U^{\varepsilon}, U^{\varepsilon})] \tag{14}$$

and we can use the thoughts given in the above Gedankenexperiment when $\varepsilon \to 0$ to evaluate the appropriate load-scaling factor.

Lovadina [14] investigated the asymptotic behavior of the strain energy of shells by means of real interpolation theory and established (under certain conditions) the relation

$$\lim_{\varepsilon\to 0} R(\varepsilon) = \frac{\rho - 1}{2}, \tag{15}$$

where $R(\varepsilon)$ denotes the proportion of bending strain energy

$$R(\varepsilon) = \frac{\varepsilon^3 A_{\mathrm{b}}(U^{\varepsilon}, U^{\varepsilon})}{\varepsilon^3 A_{\mathrm{b}}(U^{\varepsilon}, U^{\varepsilon}) + \varepsilon A_{\mathrm{m}}(U^{\varepsilon}, U^{\varepsilon})}. \tag{16}$$

Eq. (15) can be used to calculate the proper load-scaling factor for a shell from the proportion of bending strain energy to total strain energy stored in the shell; and, vice versa, if ρ is known, the bending energy as a proportion of the total strain energy can be calculated.

2.5. Remarks on finite element schemes

To this point, we reviewed some general theory regarding the asymptotic behavior of shell mathematical models. We next might ask whether, as the thickness of a shell structure decreases, shell finite element discretizations can accurately calculate the correct various asymptotic behaviors. To test finite element schemes for this purpose, we need a special series of benchmark problems, which reflect the various asymptotic behaviors of shell mathematical models.

The usual heretofore performed benchmark analyses are not sufficiently comprehensive and deep. The solutions provide only a few displacement or stress values at one or two locations of the structure as reference values, and just one shell thickness is considered. Thus, the results cannot reflect the complete behavior of the finite element schemes, which should be tested on bending-dominated, membrane-dominated, and mixed state problems as the shell thicknesses decrease [4].

A major difficulty in the development of shell finite elements is the locking phenomenon for non-inhibited shells. When the subspaces of the finite element approximations do not approximate the pure bending displacement fields in a sufficiently rich manner, membrane and shear locking, in global and local forms, occur. Then, as the shell thickness decreases, the finite element solution convergence rate deteriorates drastically, and in the worst case the solution tends to a zero displacement field.

An ideal finite element solution scheme is locking-free, satisfies the ellipticity and consistency conditions and provides optimal convergence [10]. To establish whether a given shell finite element procedure is effective, numerical tests need to be performed, and these include the inf–sup test and the solution of well-chosen benchmark problems [4,15–17]. The solutions given in the next section are valuable in providing basic information regarding some shell problems, and therefore for the selection of appropriate benchmark tests.

3. Asymptotic analysis by numerical experiments

In this section, we perform the asymptotic analysis of three different shell problems; the original Scordelis–Lo roof shell problem, a modified (here proposed) Scordelis–Lo roof shell problem and the partly clamped hyperbolic paraboloid shell problem. The three shell problems are, respectively, a mixed, membrane-dominated and bending-dominated problem.

Due to the difficulty of reaching analytical solutions for these problems, finite element solutions based on fine meshes are given. The MITC 4-node shell finite element implemented by degenerating the three-dimensional continuum to shell behavior is used for the numerical experiments [10]. Hence the finite element discretization, as used in this study, actually provides solutions of the "basic shell model" identified and analyzed by Chapelle and Bathe [5,18]. However, as shown in these references, when the shell thickness decreases, the basic shell mathematical model converges to the Naghdi model, and hence the above discussion regarding asymptotic behaviors is directly applicable.

The results of the analyses show the asymptotic behaviors of the shell problems with respect to deformations, energy distributions, layers and load-scaling factors, as the thicknesses of the considered shell structures become small. In the numerical solutions we decreased ϵ to very small values (up to 10^{-6}), impractical as it seems, in order to identify as closely as possible the limit behaviors.

3.1. Original Scordelis–Lo roof shell problem

We consider the original Scordelis–Lo roof shell problem as an example of an asymptotically mixed case. The problem is described in Fig. 4. The shell surface is a segment of a cylinder, and hence it is a parabolic surface. The shell has zero curvature in the axial direction and a uniform curvature in the circumferential direction. The asymptotic lines are in the axial direction.

Considering the boundary conditions, at the diaphragms the two displacements in the X- and Z-directions are constrained to be zero. Pure bending is obviously inhibited for the entire area of the shell. Therefore, this problem is a membrane dominated problem provided an admissible membrane loading is used ($G \in \mathscr{V}'_{\mathrm{m}}$). However, in the original version of this problem, considered in this section, the shell is subjected to self-weight loading, see Fig. 4, which corresponds to a non-admissible membrane loading ($G \notin \mathscr{V}'_{\mathrm{m}}$), as proven in Ref. [4].

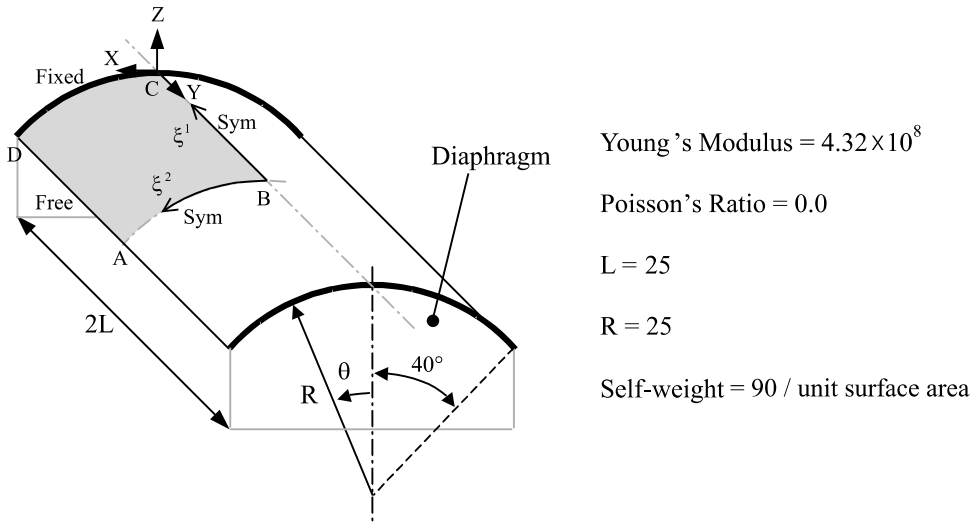

Fig. 4. Original Scordelis–Lo roof shell problem.

Table 2
Scale coefficients $q_0(\varepsilon,\mu)$ for generating scaled loadings

ε $(=t/L)$	$F\propto\varepsilon$, $\mu=1$	$F\propto\varepsilon^2$, $\mu=2$	$F\propto\varepsilon^3$, $\mu=3$
0.01	1.0E + 00	1.0E + 00	1.0E + 00
0.001	1.0E − 01	1.0E − 02	1.0E − 03
0.0001	1.0E − 02	1.0E − 04	1.0E − 06
0.00001	1.0E − 03	1.0E − 06	1.0E − 09
0.000001	1.0E − 04	1.0E − 08	1.0E − 12

Note that, of course, the second and third columns of the table can directly be inferred from the first column.

An analytical solution does not exist for this problem. The reference value representing the (total) response in benchmark solutions is the Z-directional deflection at the midpoint of the free edge (point A). The deflection at point A calculated using a very fine mesh is 0.3024 when $t = 0.25$.

Due to symmetry, we can limit our calculations to the shaded region $ABCD$. We use a 72×72 element mesh for all Scordelis–Lo roof shell solutions which is sufficiently fine to perform the asymptotic analysis of these problems.

The scaled loadings, q, used are given by the factor $q_0(\varepsilon,\mu)$ in Table 2,

$$q = q_0(\varepsilon,\mu)\times 90. \tag{17}$$

Table 3 shows the scaled calculated total strain energy of the quarter shell

$$E_0(\varepsilon,\mu) = \frac{E(\varepsilon,\mu)}{q_0(\varepsilon,\mu)} \tag{18}$$

and the corresponding proportion of bending energy as ε becomes very small. The table shows that the scaled strain energy corresponding to $F\propto\varepsilon$ increases, while the scaled strain energies corresponding to $F\propto\varepsilon^2$ and $F\propto\varepsilon^3$ decrease. This means that the proper load-scaling factor of the considered shell problem lies between 1.0 and 2.0, and hence, of course, this shell problem is a mixed problem. In accordance with this observation, the proportion of bending energy, $R(\varepsilon)$ in Eq. (16), asymptotically converges to a value between 0.0 and 0.5.

Using these results, we can directly graphically calculate the proper load-scaling factor using Fig. 5(a). As

Table 3
Scaled strain energy for the original Scordelis–Lo roof shell problem ($E_0(\varepsilon,\mu)$)

ε $(=t/L)$	$F\propto\varepsilon$	$F\propto\varepsilon^2$	$F\propto\varepsilon^3$	$R(\varepsilon)$
0.01	1.20892E + 03	1.20892E + 03	1.20892E + 03	0.522154
0.001	6.99828E + 03	6.99828E + 02	6.99828E + 01	0.399277
0.0001	3.89610E + 04	3.89610E + 02	3.89610E + 00	0.367219
0.00001	2.11544E + 05	2.11544E + 02	2.11544E − 01	0.366451
0.000001	1.13502E + 06	1.13502E + 02	1.13502E − 02	0.362567

Note that, of course, the second and third columns of the table can directly be inferred from the first column.

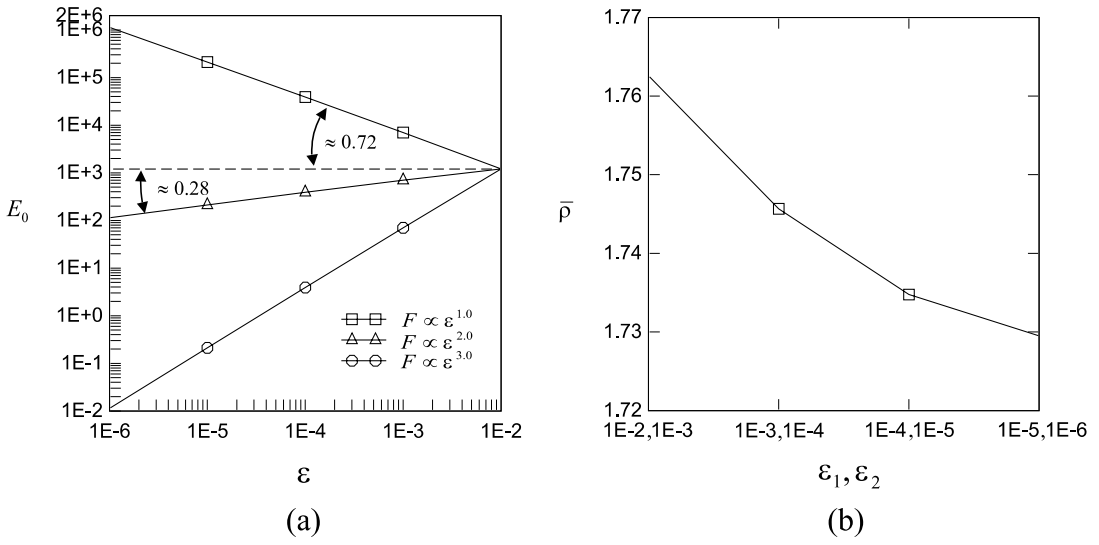

Fig. 5. The graphical evaluation of the proper load-scaling factor for the original Scordelis–Lo roof shell problem (a) scaled strain energy, (b) calculated load-scaling factor using Eq. (19).

noted in the Gedankenexperiment, if the proper load-scaling factor ρ is used as μ for the scaled loading, the slope of the line corresponding to the scaled energy is zero. This zero slope corresponds to a value of $\rho \simeq 1.72$.

A more direct way to calculate the proper load-scaling factor is to use a constant loading ($F \propto \varepsilon^0$) and Eq. (13). Then, using two different strain energies corresponding to two different thicknesses, it is possible to estimate the proper load-scaling factor as

$$\bar{\rho} = -\frac{\log E(\varepsilon_1) - \log E(\varepsilon_2)}{\log \varepsilon_1 - \log \varepsilon_2}, \tag{19}$$

in which $E(\varepsilon_1)$ and $E(\varepsilon_2)$ are, respectively, the total strain energies corresponding to ε_1 and ε_2 when a constant loading is applied. The proper load-scaling factor ρ is the limit value of Eq. (19) as the thickness approaches zero:

Table 4
The load-scaling factor calculated by the total strain energies corresponding to constant loading for the original Scordelis–Lo roof shell problem

ε $(=t/L)$	Total energy ($F \propto \varepsilon^0$)	$\bar{\rho}$
0.01	1.20892E + 03	
		1.76259
0.001	6.99828E + 04	
		1.74564
0.0001	3.89610E + 06	
		1.73477
0.00001	2.11544E + 08	
		1.72960
0.000001	1.13502E + 10	

Table 5
The angular distance d measured from the free edge to the first peak of the normalized deflection for the original Scordelis–Lo roof shell problem

Thickness t	Computed distance d	Distance d by formula $d = 5.35L^{0.75}t^{0.25}$, $L = 25$
0.25	40.0000	42.2955
0.025	23.3333	23.7845
0.0025	13.3333	13.3750
0.00025	7.77778	7.52132
0.000025	4.44444	4.22954

Note that the actual distance is $d\pi R/180$.

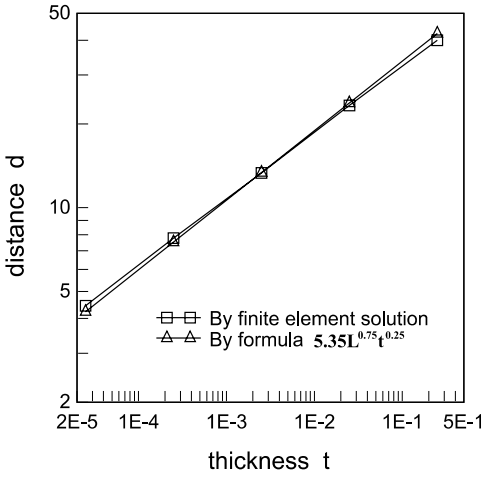

Fig. 7. The free edge boundary layer width for the original Scordelis–Lo roof shell problem.

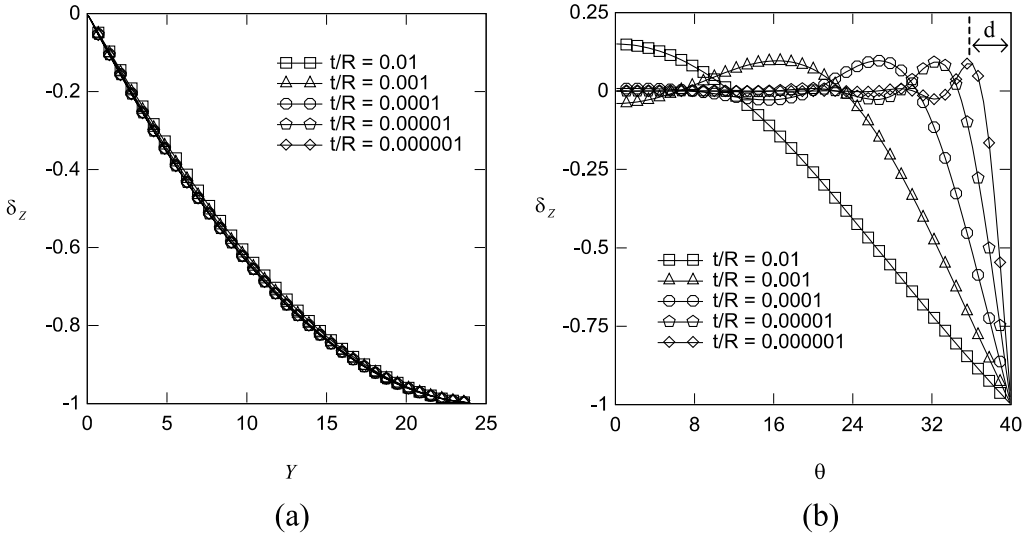

Fig. 6. The normalized deflection for the original Scordelis–Lo roof shell problem (a) along DA, (b) along BA.

$$\rho = \lim_{\varepsilon_1,\varepsilon_2 \to 0} \bar{\rho}. \tag{20}$$

Table 4 and Fig. 5(b) show that the values calculated by Eq. (19) asymptotically converge to the proper load-scaling factor ρ. Note also that just two points to define the straight line(s) in Fig. 5(a) and to calculate $\bar{\rho}$ in Eq. (19) would in practice be sufficient.

The load-scaling factor ρ calculated by Lovadina's equation, Eq. (15), is 1.725134 when $\varepsilon = 0.000001$, which is almost the same result. It requires some computations to extract the bending energy from the total strain energy of the considered shell problem. However, once ρ is known from Fig. 5 the bending energy can directly be calculated.

Figs. 6(a) and (b) show the deflections along the sections DA and BA in Fig. 4. These results are Z-directional deflections normalized by the magnitude of deflection at point A. The normalized deflection along the section DA keeps (almost) the same shape for decreasing thickness, while the normalized deflection along the section BA shows a singular behavior at the free edge as the thickness approaches zero. The

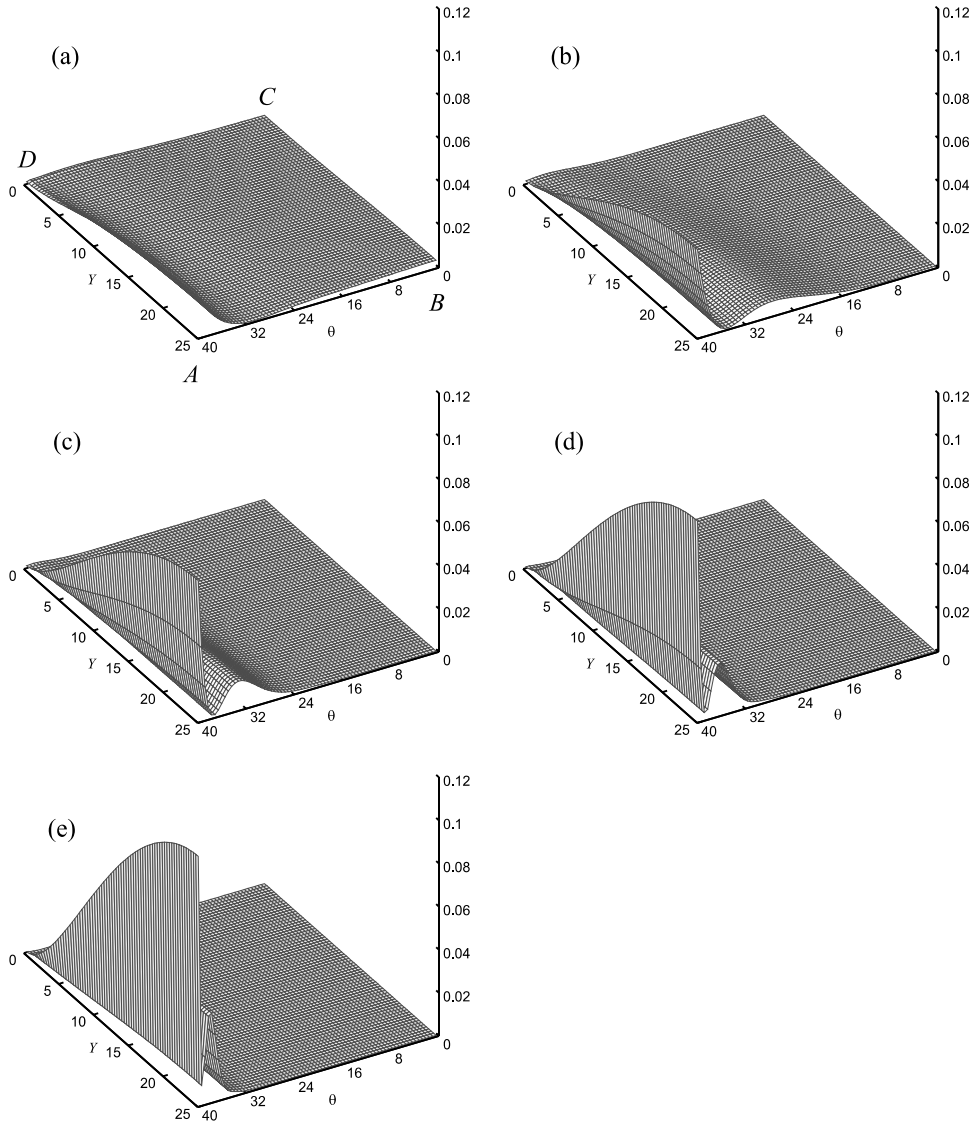

Fig. 8. Strain energy distribution for the original Scordelis–Lo roof shell problem (a) $\varepsilon = 0.01$, (b) $\varepsilon = 0.001$, (c) $\varepsilon = 0.0001$, (d) $\varepsilon = 0.00001$, (e) $\varepsilon = 0.000001$.

stress concentration is a result of the disturbance of membrane equilibrium at the free boundary edge caused by the non-admissible membrane loading, resulting in concentrating bending strain energy. This explains why this problem is asymptotically not a pure membrane problem in spite of its inhibited geometry.

It is possible to identify the characteristic length of the layer at the free boundary from Fig. 6(b). We select the angular distance measured from the free edge to the first peak of the normalized deflection corresponding to each t as the width of the layer (distance d in Fig. 6(b)). Table 5 summarizes the computed values for d and Fig. 7 shows these results graphically. We see that in this case, by curve fitting, $C \simeq 5.35$ and $1 - l \simeq 0.25$.

Finally, it is valuable to consider the asymptotic change of energy distributions. Figs. 8–10 show the energy distributions corresponding to the total strain energy, bending strain energy only and membrane strain energy only, each time given as energies per unit surface-area normalized by the total strain energy stored in the quarter shell structure.

The areas $ABCD$ in Figs. 8–10 correspond to the area $ABCD$ in Fig. 4. Fig. 8 shows that the energy becomes concentrated in the free edge boundary layer as the

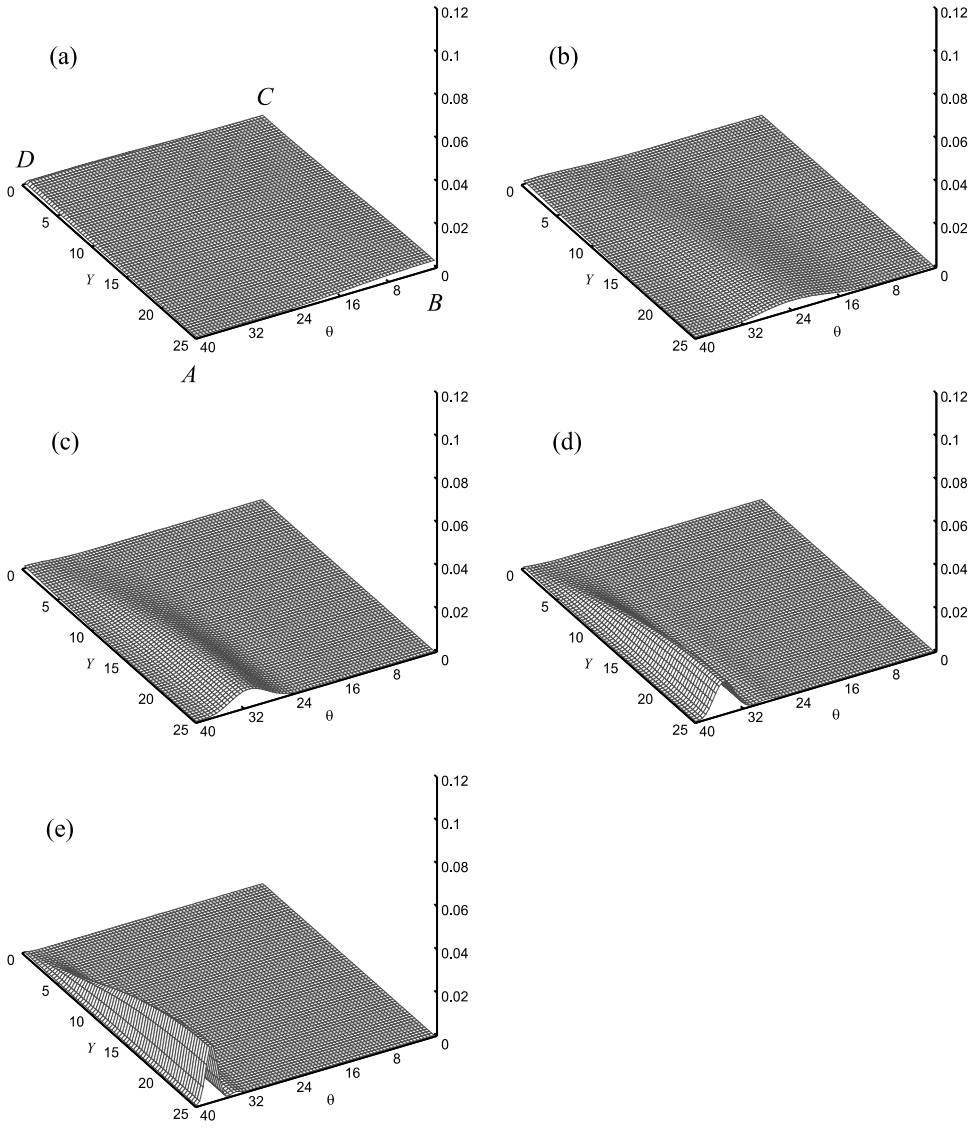

Fig. 9. Bending energy distribution for the original Scordelis–Lo roof shell problem (a) $\varepsilon = 0.01$, (b) $\varepsilon = 0.001$, (c) $\varepsilon = 0.0001$, (d) $\varepsilon = 0.00001$, (e) $\varepsilon = 0.000001$.

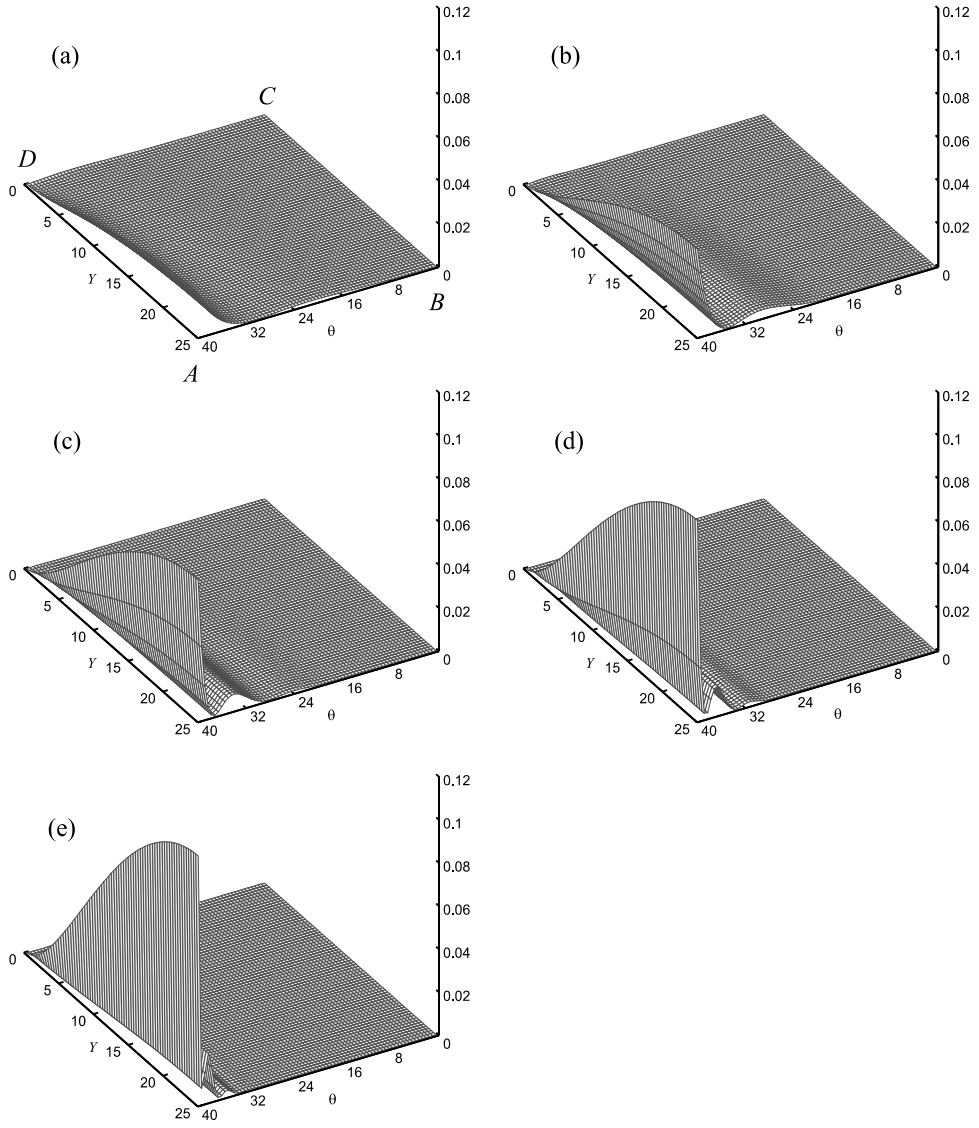

Fig. 10. Membrane energy distribution for the original Scordelis–Lo roof shell problem (a) $\varepsilon = 0.01$, (b) $\varepsilon = 0.001$, (c) $\varepsilon = 0.0001$, (d) $\varepsilon = 0.00001$, (e) $\varepsilon = 0.000001$.

thickness approaches zero. Fig. 9 shows that the bending strain energy does not asymptotically approach zero but concentrates near the free edge. Comparing this figure with Fig. 6(b), we see that the bending strain energy is concentrated around the first peak in Fig. 6(b). This prevents this shell problem from being a pure membrane problem and keeps a balance of membrane and bending strain energies. Clearly, it is the concentration of the bending strain energy in the free edge boundary layer that results in the mixed state of the asymptotic behavior. Fig. 10 shows that the membrane strain energy is also asymptotically concentrated near the free edge.

3.2. Modified Scordelis–Lo roof shell problem

In the original Scordelis–Lo roof shell problem, the shell is subjected to a uniformly distributed loading which does not correspond to a membrane admissible loading. This condition renders the problem to be an asymptotically mixed shell problem. Here we are interested in changing this problem into a membrane-dominated problem by using another applied loading instead of the uniform loading without changing the geometry and constraints. To achieve this objective, the newly applied loading should not induce a concentration of

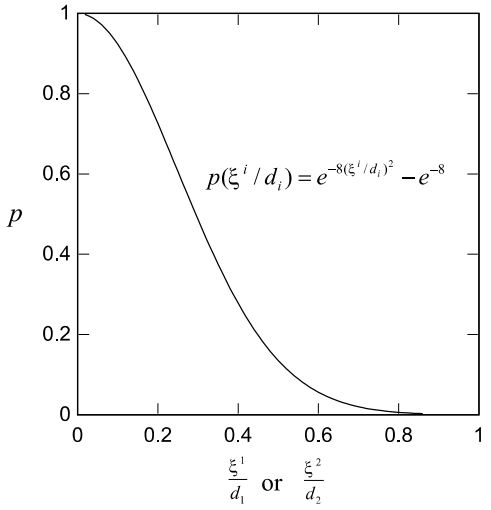

Fig. 11. Distribution of loading.

strain energy at the free boundary. Fig. 11 shows the profile of the proposed loading using the ξ^1 and ξ^2 coordinates defined in Fig. 4.

The new distributed loading on the 2D shell surface is acting into the negative Z-direction with magnitude

$$q(\xi^1, \xi^2) = q_0(\varepsilon, \mu)\{e^{-8(\xi^1/d_1)^2} - e^{-8}\}\{e^{-8(\xi^2/d_2)^2} - e^{-8}\}, \tag{21}$$

where $q_0(\varepsilon, \mu)$ is the scaling coefficient for generating the scaled applied loading given in Table 2, and d_1 and d_2 are, respectively, the distances measured along ξ^1 from B to C and along ξ^2 from B to A in Fig. 4.

Table 6 and Fig. 12(a) show that the scaled strain energy corresponding to $F \propto \varepsilon$ becomes a constant value whereas the scaled strain energies corresponding to $F \propto \varepsilon^2$ and $F \propto \varepsilon^3$ decrease and approach zero. Therefore, the proper load-scaling factor of this shell problem is clearly 1.0. Accordingly, also, the value of $R(\varepsilon)$ in

Table 6
Scaled strain energy for the modified Scordelis–Lo roof shell problem ($E_0(\varepsilon, \mu)$)

ε $(=t/L)$	$F \propto \varepsilon$	$F \propto \varepsilon^2$	$F \propto \varepsilon^3$	$R(\varepsilon)$
0.01	1.84299E − 03	1.84299E − 03	1.84299E − 03	0.363274
0.001	5.13474E − 03	5.13474E − 04	5.13474E − 05	0.151134
0.0001	7.49566E − 03	7.49566E − 05	7.49566E − 07	0.021661
0.00001	7.69900E − 03	7.69900E − 06	7.69900E − 09	0.000374
0.000001	7.70523E − 03	7.70523E − 07	7.70523E − 11	0.000040

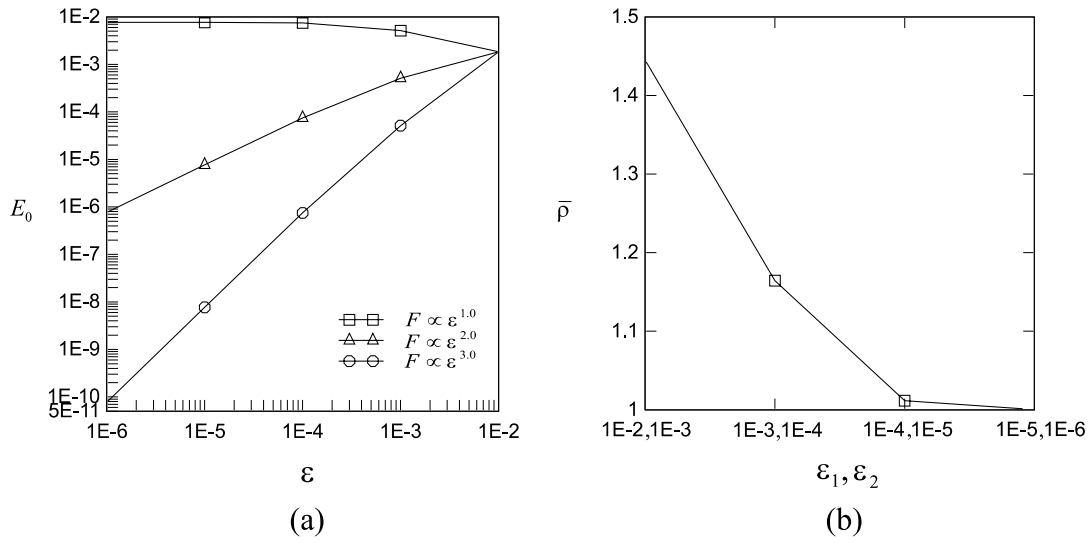

Fig. 12. The graphical evaluation of the proper load-scaling factor for the modified Scordelis–Lo roof shell problem (a) scaled strain energy, (b) calculated load-scaling factor using Eq. (19).

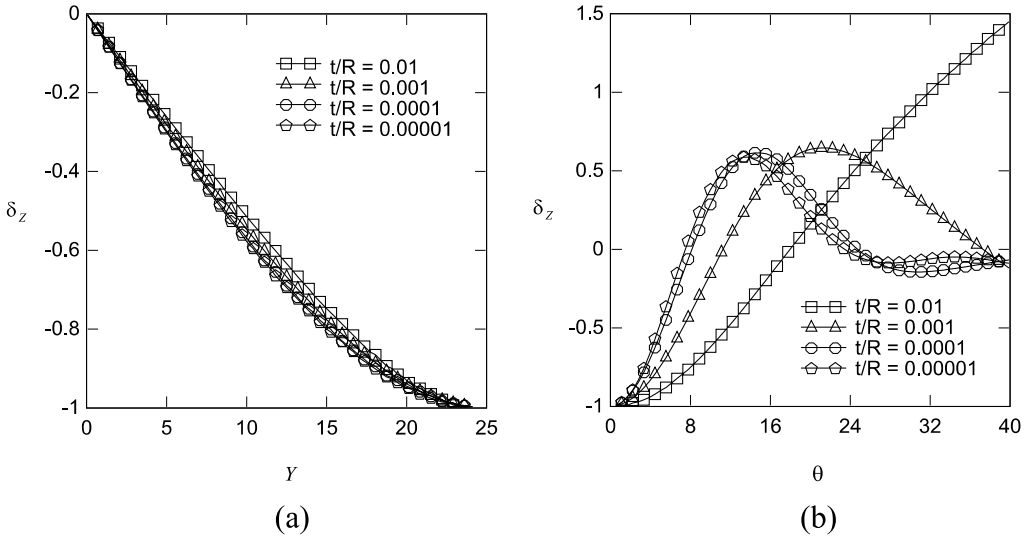

Fig. 13. The normalized deflection for the modified Scordelis–Lo roof shell problem (a) along *CB*, (b) along *BA*.

Table 6 tends to zero. In Fig. 12(b), the load-scaling factor calculated by Eq. (19) converges to 1.0 as the thickness decreases. All of these results mean that in this problem, asymptotically only membrane strain energy is encountered.

Figs. 13(a) and (b) show the normalized deflections along the sections *CB* and *BA* in Fig. 4. The results in the figures are normalized by the magnitude at point *B*. The normalized deflections along the section *CB* have almost the same shape for various thicknesses, while the normalized deflections along the section *BA* converge to a specific limit shape as the thickness decreases. No strain layer is observed in these two figures.

Fig. 14 shows [1] that the strain energy becomes large near point *B* as the thickness decreases, but the overall energy distribution does not vary significantly once ε has reached the value of 0.0001. Considering Fig. 15, we see that the bending strain energy asymptotically vanishes over the complete shell surface, while Fig. 16 shows that the distribution of membrane strain energy asymptotically converges to the distribution of the total strain energy shown in Fig. 14.

These results show that this is a membrane-dominated shell problem and that merely the use of the new load distribution induced a dramatic change in the asymptotic behavior.

[1] For better readability, the results in Figs. 14–16 are plotted using a 36×36 element mesh, but these are identical to the results obtained using the 72×72 mesh.

3.3. Partly clamped hyperbolic paraboloid shell problem

This shell problem is classified as a bending dominated problem. The problem was suggested in Ref. [4] as a good problem to test finite element procedures as to whether or not a scheme locks. The surface is defined as

$$\begin{pmatrix} X \\ Y \\ Z \end{pmatrix} = L \begin{pmatrix} \xi^1 \\ \xi^2 \\ (\xi^1)^2 - (\xi^2)^2 \end{pmatrix}; \quad (\xi^1, \xi^2) \in \left[-\frac{1}{2}, \frac{1}{2} \right]^2, \tag{22}$$

and clamped along the side $Y = -L/2$. The structure is loaded by its self-weight.

By symmetry, only one half of the surface needs to be considered in the analysis (the shaded region *ABCD* in Fig. 17), with clamped boundary conditions along *BC* and symmetry conditions along *AB*. As mentioned already, this shell problem has a triangular inhibited area defined by the points *C*, *B*, and the midpoint of *BA*.

For the finite element analysis we use a uniform 144×72 element mesh, which is considered sufficiently fine.

The scaled loading (force per unit area) for the asymptotic analysis is

$$q = q_0(\varepsilon, \mu) \times 80, \tag{23}$$

where $q_0(\varepsilon, \mu)$ is the scaling coefficient for generating the scaled applied loading and is given in Table 2.

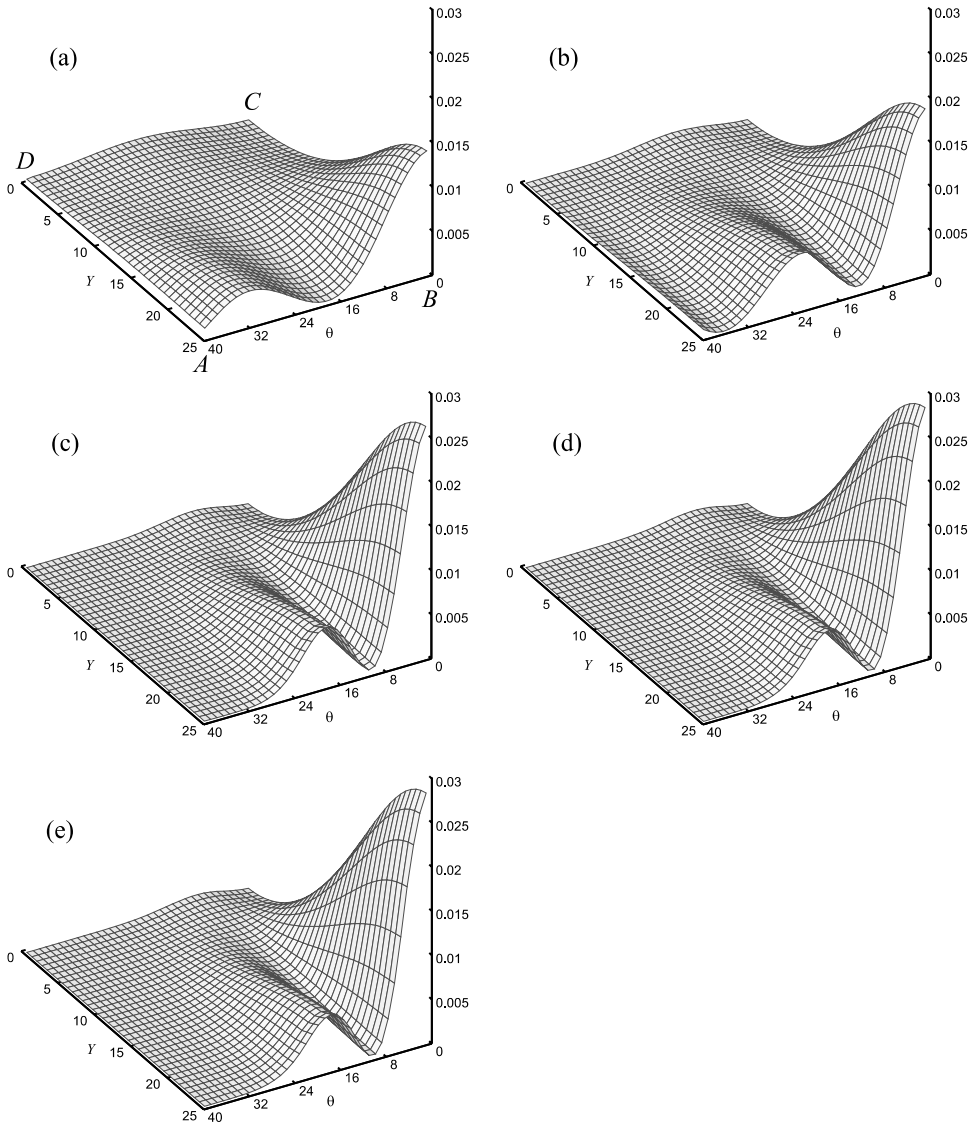

Fig. 14. Strain energy distribution for the modified Scordelis–Lo roof shell problem (a) $\varepsilon = 0.01$, (b) $\varepsilon = 0.001$, (c) $\varepsilon = 0.0001$, (d) $\varepsilon = 0.00001$, (e) $\varepsilon = 0.000001$.

We use the scaled loadings with $\mu = 1, 2, 3$. Table 7 and Fig. 18(a) show the scaled strain energies calculated in the finite element solutions. The results show that the scaled strain energies corresponding to $F \propto \varepsilon$ and $F \propto \varepsilon^2$ continuously increase, while the scaled strain energy corresponding to $F \propto \varepsilon^3$ converges to a constant value. The proportion of bending energy given by $R(\varepsilon)$ in Table 7 converges to 1.0 as the thickness of the shell decreases. In addition, the load-scaling factor calculated by Eq. (19) converges to 3.0, see Fig. 18(b). Therefore, the proper load-scaling factor of this shell problem is 3.0 which corresponds of course to a bending dominated problem.

Figs. 19(a) and (b) show the normalized Z-directional deflections along the sections BA and AD. The deflections are normalized by the magnitudes at point A and point D, respectively. The two figures show that there exists a specific limit displacement shape.

Figs. 20–22 illustrate [2] the asymptotic changes in normalized total strain energy, bending energy and

[2] For better readability, the results in Figs. 20–22 are plotted using a 72×36 element mesh, but these are identical to the results obtained using the 144×72 mesh.

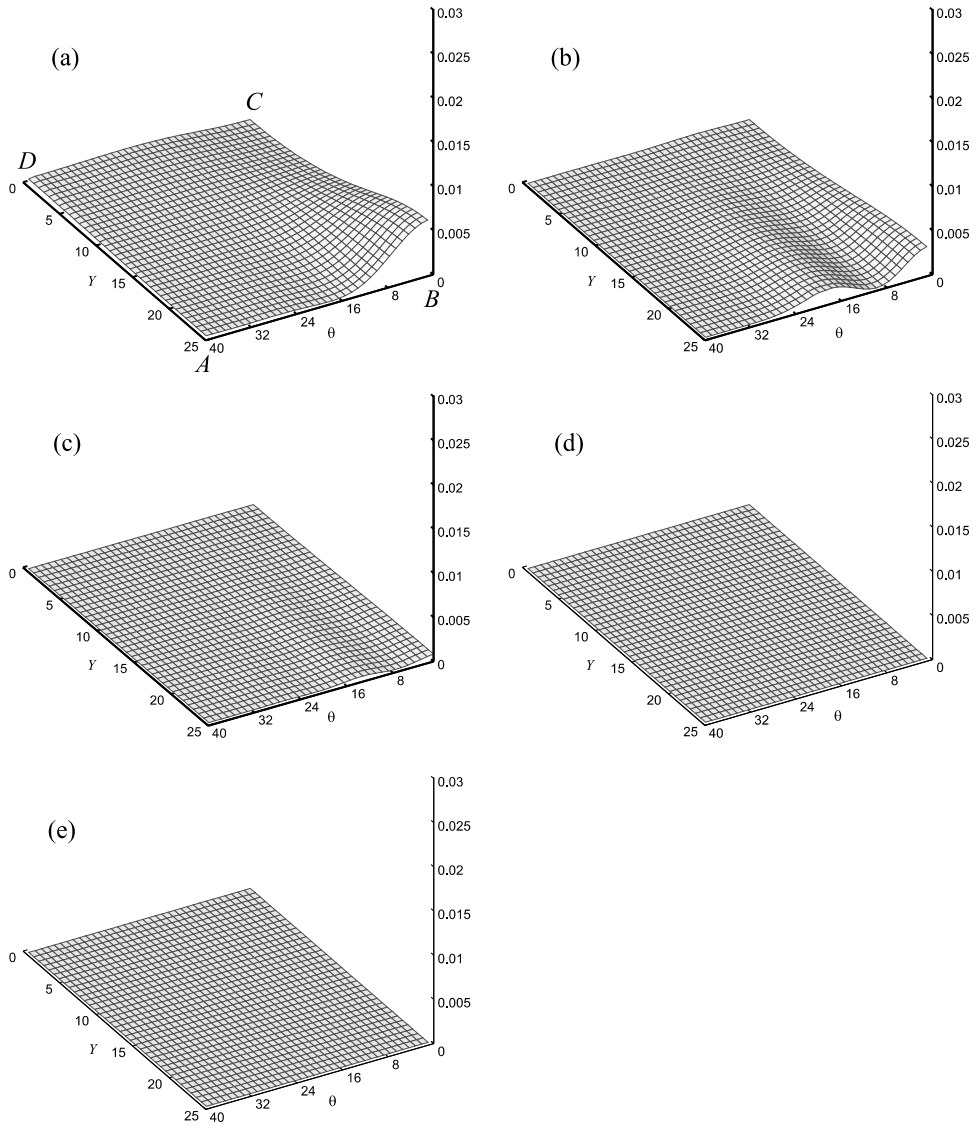

Fig. 15. Bending energy distribution for the modified Scordelis–Lo roof shell problem (a) $\varepsilon = 0.01$, (b) $\varepsilon = 0.001$, (c) $\varepsilon = 0.0001$, (d) $\varepsilon = 0.00001$, (e) $\varepsilon = 0.000001$.

membrane energy. We note that asymptotically the distributions of bending and total strain energies are the same. The strain energy in the inhibited area is very small and there is a significant strain energy concentration at the boundary between the inhibited area and the non-inhibited area. This energy concentration is due to the discontinuity in geometric rigidity between these areas. The observed inner layers are located along the asymptotic lines of the shell starting at the corners.

Finally, we would like to mention that it would be valuable to further study the strain concentration at the corner point C which in these numerical solutions disappears as the thickness becomes small.

4. Concluding remarks

The objective of this paper is to illustrate how an asymptotic analysis of a shell structure can be performed. Three shell problems were analyzed and some detailed results are presented.

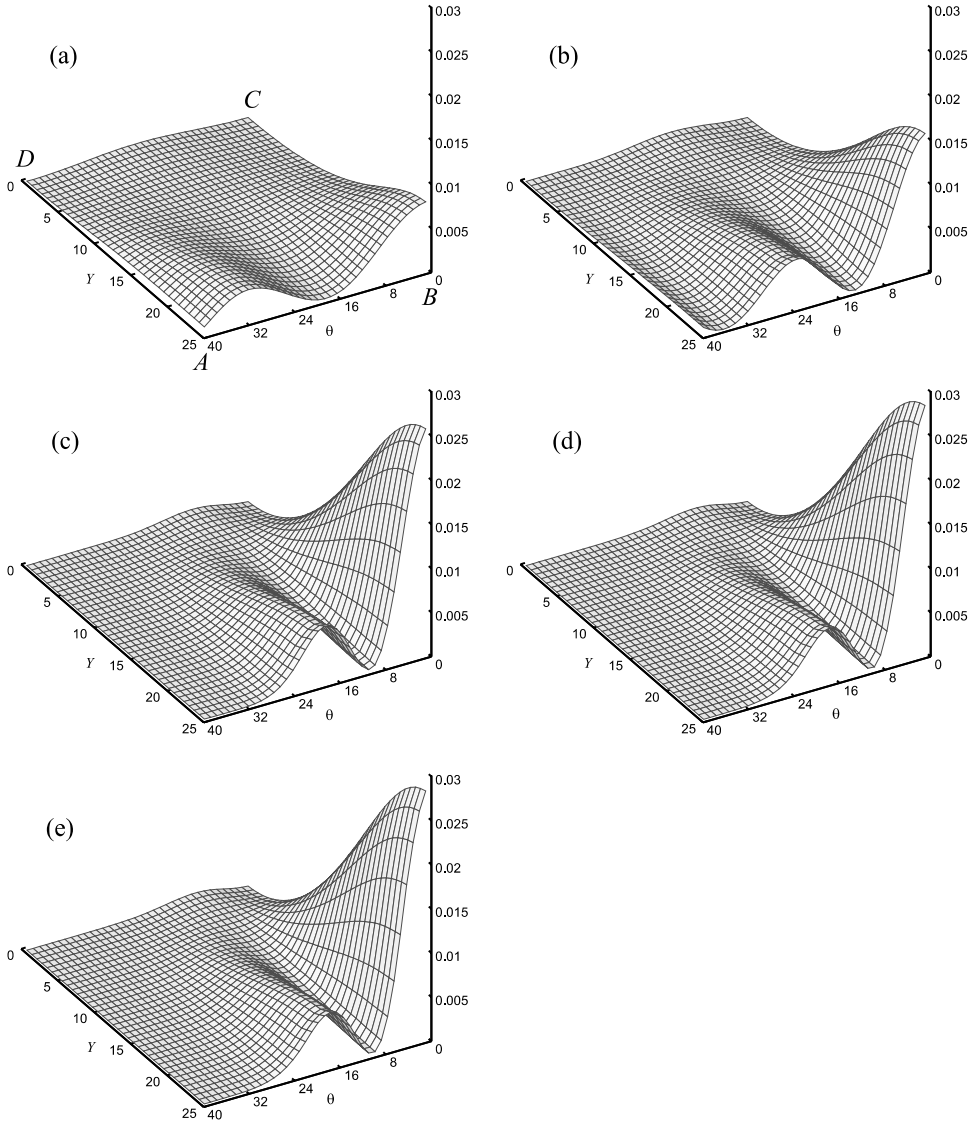

Fig. 16. Membrane energy distribution for the modified Scordelis–Lo roof shell problem (a) $\varepsilon = 0.01$, (b) $\varepsilon = 0.001$, (c) $\varepsilon = 0.0001$, (d) $\varepsilon = 0.00001$, (e) $\varepsilon = 0.000001$.

Through this study, we identified boundary layers, characteristic lengths, and proper load-scaling factors, and observed the asymptotic change of energy distributions. Specifically, we observed that the proper load-scaling factor calculated by several schemes can be used as an indicator of the asymptotic behavior of shell structures.

The study provides valuable reference values for benchmark problems to test the robustness of shell finite elements and valuable information for engineers designing shell structures.

Regarding the three considered shell problems, we have made the following observations:

- The original Scordelis–Lo roof shell problem is asymptotically a mixed problem. Even though pure bending is obviously inhibited in the entire shell, the non-admissible membrane loading (the shell self-weight) induces a concentrated strain energy layer at the free edge with bending strain energy. The proper load-scaling factor of the problem is about 1.72.

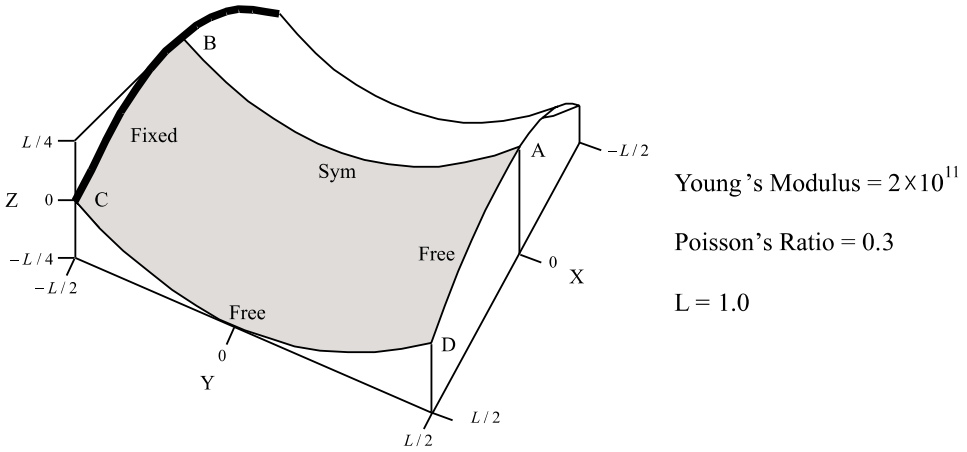

Fig. 17. Partly clamped hyperbolic paraboloid shell problem.

Table 7
Scaled strain energy for the partly clamped hyperbolic paraboloid shell problem ($E_0(\varepsilon,\mu)$)

ε $(=t/L)$	$F \propto \varepsilon$	$F \propto \varepsilon^2$	$F \propto \varepsilon^3$	$R(\varepsilon)$
0.01	8.37658E − 04	8.37658E − 04	8.37658E − 04	0.876383
0.001	5.48614E − 02	5.48614E − 03	5.48614E − 04	0.937673
0.0001	4.46665E + 00	4.46665E − 02	4.46665E − 04	0.969496
0.00001	4.05017E + 02	4.05017E − 01	4.05017E − 04	0.986142
0.000001	3.88468E + 04	3.88468E + 00	3.88468E − 04	0.994201

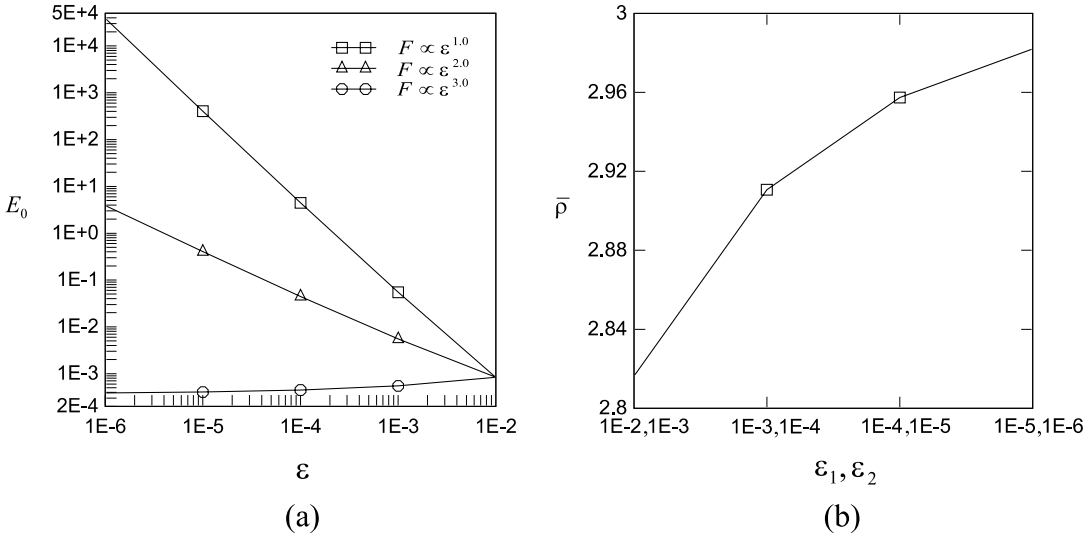

Fig. 18. The graphical evaluation of the proper load-scaling factor for the partly clamped hyperbolic paraboloid shell problem (a) scaled strain energy, (b) calculated load-scaling factor using Eq. (19).

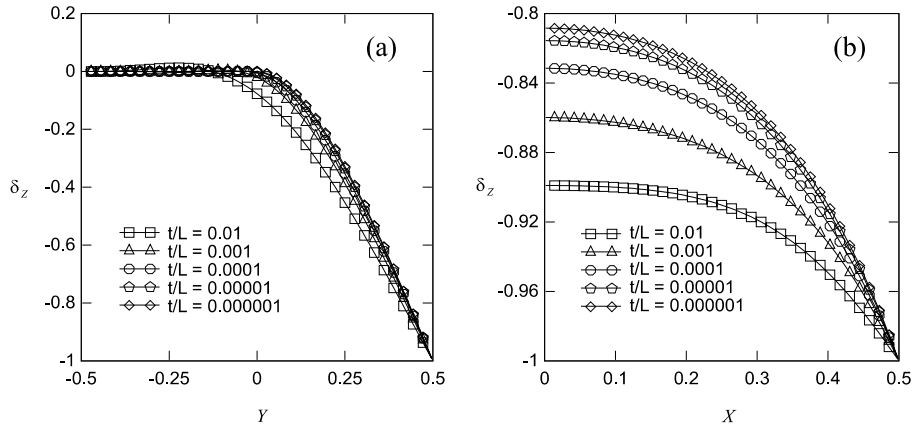

Fig. 19. The normalized deflection for the partly clamped hyperbolic paraboloid shell problem (a) along BA, (b) along AD.

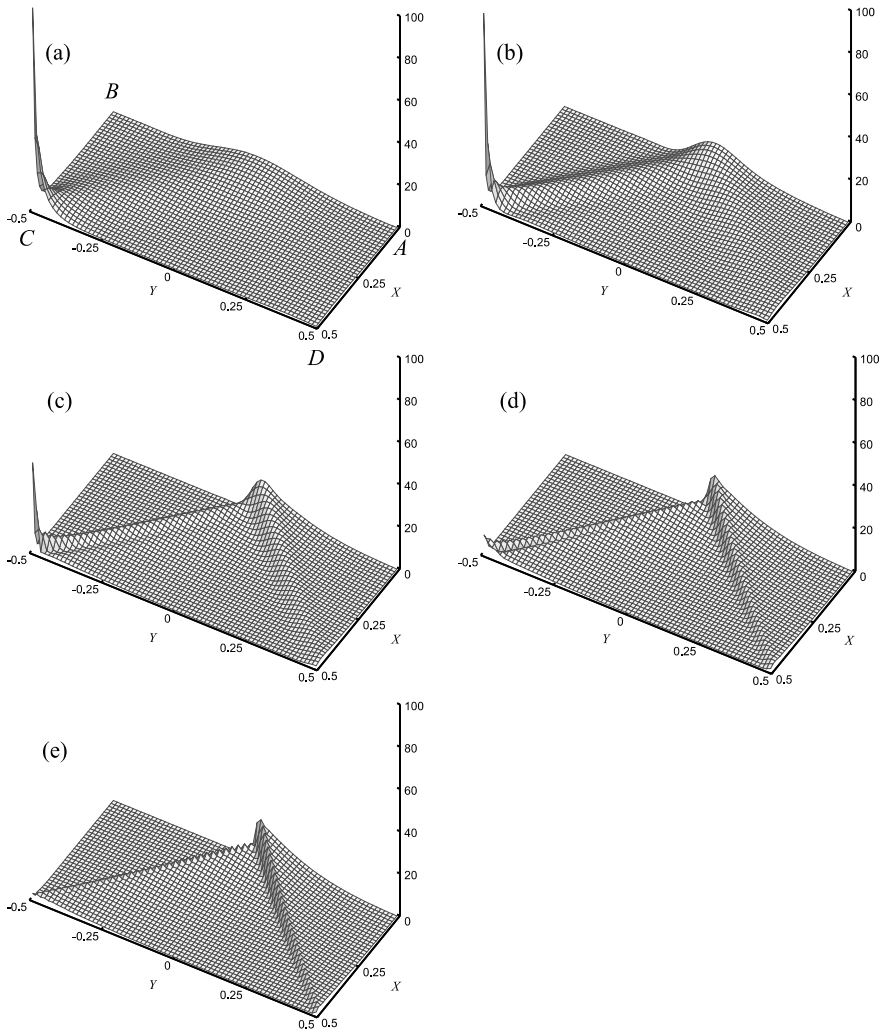

Fig. 20. Strain energy distribution for the partly clamped hyperbolic paraboloid shell problem (a) $\varepsilon = 0.01$, (b) $\varepsilon = 0.001$, (c) $\varepsilon = 0.0001$, (d) $\varepsilon = 0.00001$, (e) $\varepsilon = 0.000001$.

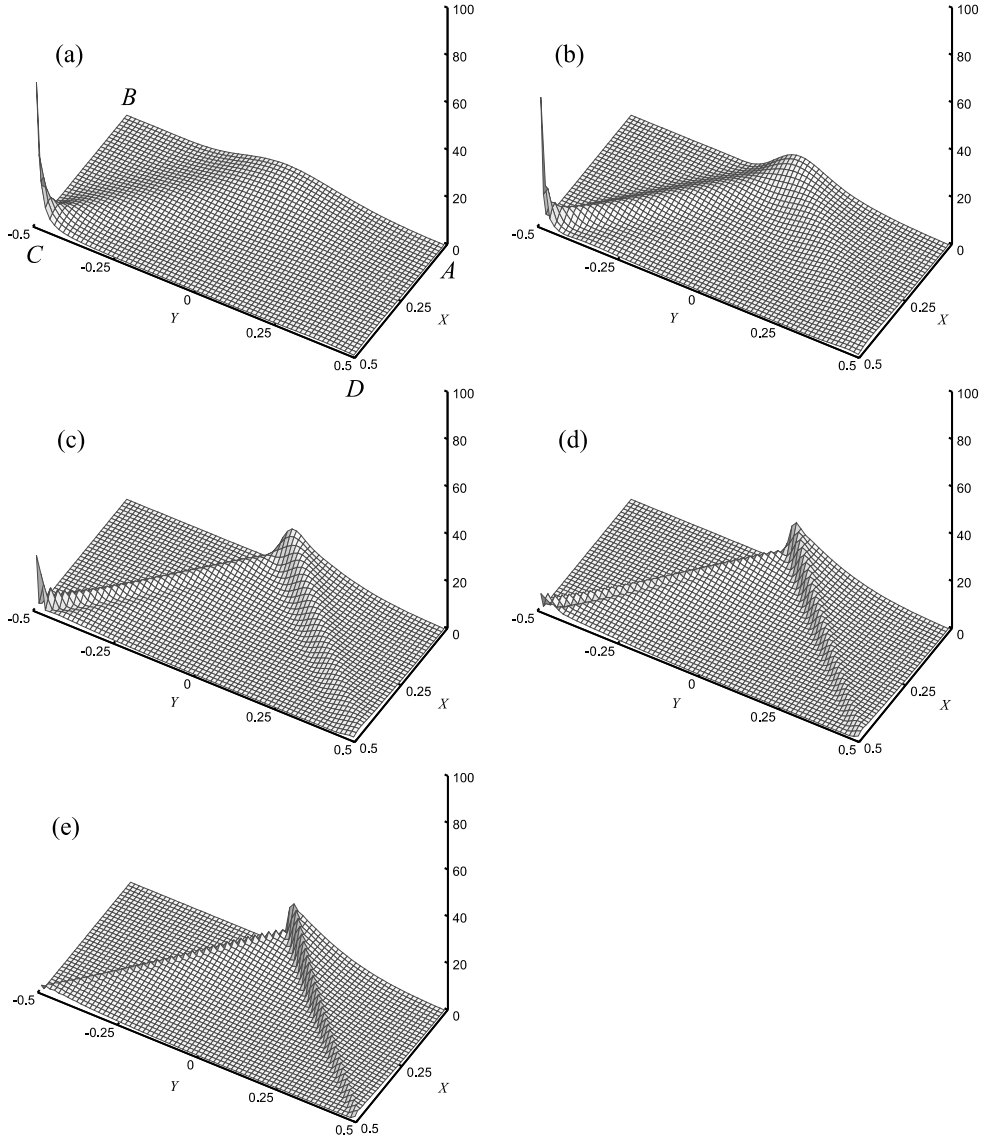

Fig. 21. Bending energy distribution for the partly clamped hyperbolic paraboloid shell problem (a) $\varepsilon = 0.01$, (b) $\varepsilon = 0.001$, (c) $\varepsilon = 0.0001$, (d) $\varepsilon = 0.00001$, (e) $\varepsilon = 0.000001$.

- The proposed modified Scordelis–Lo roof shell problem is asymptotically a membrane-dominated problem. Merely the use of a new load distribution in the original Scordelis–Lo roof shell problem induces a dramatic change of asymptotic behavior. This example illustrates not only how sensitive shell structures are but also how membrane-dominated shells behave.
- The partly clamped hyperbolic paraboloid shell problem is a representative bending-dominated problem. The solution results illustrate the asymptotic behavior of bending-dominated shells, and also show how internal concentrated energy layers can develop in a shell structure.

Acknowledgements

We are thankful to D. Chapelle, INRIA-Rocquencourt, France, for valuable discussions on the subject of this paper, and to C. Lovadina of the University of

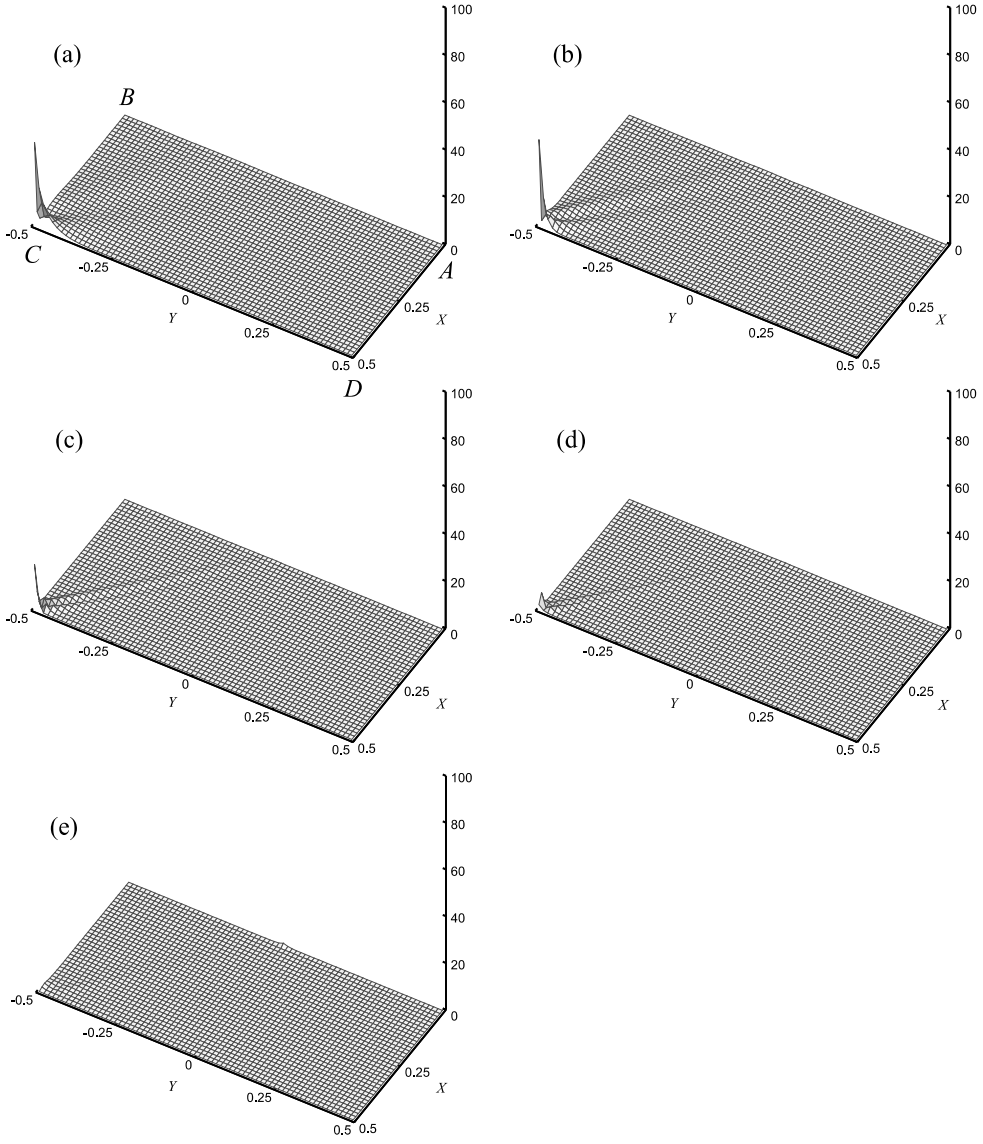

Fig. 22. Membrane energy distribution for the partly clamped hyperbolic paraboloid shell problem (a) $\varepsilon = 0.01$, (b) $\varepsilon = 0.001$, (c) $\varepsilon = 0.0001$, (d) $\varepsilon = 0.00001$, (e) $\varepsilon = 0.000001$.

Pavia, Italy, and D. Chapelle for their comments on this writing.

References

[1] Gol'denveizer AL. Theory of elastic thin shells. Oxford: Pergamon Press; 1961.
[2] Novozhilov VV. Thin shell theory. Groningen: Noordhoff Publishing; 1970.
[3] Flügge W. Stresses in shells, 2nd ed. Berlin: Springer; 1973.
[4] Chapelle D, Bathe KJ. Fundamental considerations for the finite element analysis of shell structures. Comput Struct 1998;66(1):19–36.
[5] Chapelle D, Bathe KJ. The finite element analysis of shells. Berlin: Springer-Verlag, in press.
[6] Pitkäranta J, Leino Y, Ovaskainen O, Piila J. Shell deformation states and the finite element method: a benchmark study of cylindrical shells. Comput Meth Appl Mech Eng 1995;128:81–121.
[7] Hakula H, Leino Y, Pitkäranta J. Scale resolution, locking, and high-order finite element modelling of shells. Comput Meth Appl Mech Eng 1996;133:157–82.

[8] Malinen M, Pitkäranta J. A benchmark study of reduced-strain shell finite elements: quadratic schemes. Int J Numer Meth Eng 2000;48:1637–71.
[9] Blouza A, Brezzi F, Lovadina C. Sur la classification des coques linéairement élastiques. CR Acad Sci Paris, Série I 1999;328:831–6.
[10] Bathe KJ. Finite element procedures. New York: Prentice-Hall; 1996.
[11] Rutten HS. Theory and design of shells on the basis of asymptotic analysis. Rutten and Kruisman Consulting Engineers; 1973.
[12] Farshad M. Design and analysis of shell structures. Boston: Kluwer Academic Publishers; 1992.
[13] Sanchez-Palencia E. General properties of thin shell solutions, propagation of singularities and their numerical incidence. In: Bathe KJ, editor. Computational Fluid and Solid Mechanics. Amsterdam: Elsevier Science; 2001. p. 454–5.
[14] Lovadina C. Energy estimates for linear elastic shells. In: Bathe KJ, editor. Computational Fluid and Solid Mechanics. Amsterdam: Elsevier Science; 2001. p. 330– 1.
[15] Bathe KJ. The inf–sup condition and its numerical evaluation for mixed finite element methods. Comput Struct 2001;79:243–52, 971.
[16] Bathe KJ, Iosilevich A, Chapelle D. An inf–sup test for shell finite elements. Comput Struct 2000;75:439–56.
[17] Bathe KJ, Iosilevich A, Chapelle D. An evaluation of the MITC shell elements. Comput Struct 2000;75: 1–30.
[18] Chapelle D, Bathe KJ. The mathematical shell model underlying general shell elements. Int J Numer Meth Eng 2000;48:289–313.